An ultrafast rechargeable lithium metal battery

Journal Name

COMMUNICATION

An Ultrafast Rechargeable Lithium Metal Battery

Xiang Li,[a, b, c] Shaohua Guo,[a]* Han Deng,[b, c] KeZhu Jiang,[a] Yu Qiao,[b, c] Masayoshi Ishida[b] and Haoshen Zhou[a, b, c]*

Rechargeable lithium metal battery has been regarded as one of the most attractive high-energy-density batteries due to the large specific capacity and the lowest reduction potential of metallic lithium. However, the uncontrolled Li dendrite growth and resulted unstable interfaces during the repeated Li plating/stripping lead to the severe safety issue and short cycling life, which would be aggravated especially at a high current density. Herein, we present an organic/inorganic composite protective layer via pretreating a lithium metal in $Mn(NO_3)_2$-containing carbonate electrolyte, not only enabling the stable lithium deposition and formation with the prolonged cycle life, but also delivering a record high rate of 20 mA cm^{-2} with the minimized overpotential of 60 mV in the symmetric lithium cells. Results indicate that such an artificial protective film could effectively prolong the cycling life of Li|Cu cells, and greatly improve the comprehensive electrochemical performance of the Li|LiMn$_2$O$_4$ cell. The pretreated-Li|LiMn$_2$O$_4$ cells shows outstanding cycling performance with 83% capacity retention over 200 cycles at a high rate of 2C and a high temperature of 55 ºC, and exhibits robust recovery capability with high capacity and coulombic efficiency after the cycles at 10C. These findings highlight the significance of protective layer in stabilizing Li metal anode and pave a new way for the design of high-energy batteries for practical utilization.

Lithium-ion batteries are developing widely in our lives as energy storage devices. However, the current state-of-the-art materials cannot satisfy our increasing demand in large energy storage fields such as the electronic vehicle due to their limited energy density.[1-3] Lithium metal is considered as the perfect negative electrode materials because of the highest theoretical specific capacity ($\sim$ 3860 mAh g^{-1}) and the lowest electrochemical potential (-3.04 V *vs* standard hydrogen electrode).[4, 5] Meanwhile, Li-S and Li-air systems have been regarded as the next generation high-energy alternatives precisely due to the use of Li anodes.[6-9] Although lithium metal has the excellent advantages, the unsolved issues still restrict its application, including the Li dendrite formation and unstable interfaces.[10] Lithium dendrites germinate during plating process accompanied by the uneven Li-ion flux that is caused by inhomogeneous lithium metal surface, and continuously grow up during cycling, which will finally pierce the separator, leading to the short circuit and serious security issue. Additionally, the repeated formation of SEI resulted from unstable interfaces will consume Li-ions continuously, giving rise to more and more "dead Li" (Li is isolated in the electrolyte without contact with the anode), irreversible capacity loss and low coulombic efficiency.[11, 12]

To resolve the issues as mentioned above, massive efforts are made to develop the dendrite-free and high coulombic efficiency Li metal anode. Generally, there are four exploitable strategies to protect the lithium metal electrode, improving the electrochemical performance of Li metal anode.[13-15] The first is utilizing the electrolyte additives, which can react with Li metal and thus form a stable SEI film.[16, 17] The second is the artificial SEI formed by physical or/and electrochemical method to ensure the uniform deposition of Li-ions.[18] The third is using solid electrolyte to prevent dendrite propagation.[19] The forth is introducing the porous conductive matrix to induce the uniform Li-ion flux and stable plating of Li-ions.[20] Recently, H. Yu *et al.* exhibited a self-aligned columnar structure with smooth and dendrite-free Li deposition in a carbonate-ether mixed electrolyte.[21] R. Xu *et al.* presented an artificial soft-rigid protective layer for dendrite-free Li metal anode.[22] S. Choudhury *et al.* reported a highly reversible Li metal battery based on crosslinked hairy nanoparticles, which can afford enhanced mechanical strength and good ionic conductivity.[23] L.

a.Center of Energy Storage Materials & Technology, College of Engineering and Applied Sciences, National Laboratory of Solid State Microstructures, and Collaborative Innovation Center of Advanced Microstructure, Nanjing University, Nanjing 210093, China

b.Graduate School of System and Information Engineering, University of Tsukuba, Tennoudai 1-1-1, Tsukuba, 305-8573, Japan.

c.Energy Technology Research Institute, National Institute of Advanced Industrial Science and Technology (AIST), Japan.

† Emails: shguo@nju.edu.cn, hszhou@nju.edu.cn.

Liu *et al.* employed free-standing hollow carbon fibers as the capacity container with a porous skeleton, which can suppress Li dendrite growth and achieve high coulombic efficiency.[24] Although these studies make the contribution on restricting Li dendrite growth, however, either the operation is complicated, or the performance at high current density cannot be improved manifestly.

In our report, we demonstrate a pre-treated method to improve the stability of SEI and electrochemical performance of Li-metal electrode. Lithium metal was pre-treated by immersing into the $Mn(NO_3)_2$ additive electrolyte before usage. The method has three obvious advantages: 1) the additive is common reagent and inexpensive enough because of the abundant Mn source in the earth's crust. 2) The pre-treated operation is simple and immediate. 3) The results are marvellous, especially at high current density. In symmetric cell tests, the overpotential is as small as 20 mV at 5 mA cm^{-2}. Meanwhile, the pre-treated Li metal exhibits wondrous rate performance even at the extremely high current density of 20 mA cm^{-2}. The performance is also impressive in pretreated-Li|LiMn$_2$O$_4$ cell tests at high temperature (55 ^{o}C) compared with the bare Li|LiMn$_2$O$_4$ cells, as well as in coulombic efficiency tests using copper as the counter electrode.

The operation of pre-treatment is facile, as shown in Figure 1a and 1b. Li metal was pouched on the stainless steel slightly and then immersed into the 1M LiPF$_6$ in EC/DEC (ethylene carbonate/diethyl carbonate, v: v = 1:1) electrolyte with $Mn(NO_3)_2$ additive. The electrolyte and $Mn(NO_3)_2$ additive was reduced by Li metal through chemical reaction and a black SEI film was formed fast (within 1 min) on the surface of Li metal. The SEI film was then analyzed by SEM (scanning electron microscope) after rinsing by DME (dimethoxyethane) and drying in glove box. As shown in Figure 1c, granular particles were displayed in the view, which were the tips of the nanotubes in fact, as shown in Figure 1d. An elaborate view can be seen in Figure 1e, the nanotubes were the production of the chemical reaction between Li metal and electrolyte (with additive) with the diameter of ∼ 500 nm, composing the nano-arrays. The nanotubes arrays, on one hand, generate abundant Li nucleation sites, leading to a uniform Li deposition. On the other hand, the special nanotubes arrays skeleton distinctly decreases the local current density, thereby alleviating the Li dendrite growth. Furthermore, the free space in nanotubes restricts the huge volumetric expansion in Li metal during electrochemical cycling process.[14] All the characterizations would ensure a stable SEI and dendrite-free Li deposition. In contrast, there were no nanotubes arrays formed if no additive was added into the electrolyte, as shown in Figure S1. To reveal the elements distribution of the nanotubes, EDX (energy dispersive X-ray spectroscopy) was employed, the result was shown in Figure S2. The elements of C, N, O, F and Mn distributed uniformly apart from P, demonstrating the homogeneous composition of the nanotubes. The cross-section of SEI was also carried out, with the thickness of ∼ 6 μm, as shown in Figure 1f. The SEI thickness has the relationship with both of the reacting time and the content of additive, as shown in Figure S3. To explore the composition of SEI formed in Figure

1b, XPS (X-ray photoelectron spectroscopy) was performed, as shown in Figure 1g (Li1s, N1s, and Mn2p) and Figure S4 (C1s, O1s, F1s and P2p). The composition of C, O, F, and P is in agreement with previous literature exerting similar electrolyte.[25-27] The fitted C1s spectrum shows peaks related to –C-C-, ROCO$_2$Li, and Li$_2$CO$_3$. The fitted O1s spectrum shows peaks related to C=O and C-O, which is consistent with the C1s spectrum. In addition, there is one small peak at 528.5 eV belonging to metal oxides, which is different from the SEI composition formed in the traditional electrolyte. F1s spectrum was fitted by LiF and Li$_x$PO$_y$F$_z$ with peaks located at 685.0 and 686.7 eV respectively.[25] Besides, there also exists trace quantities of Li$_x$PO$_y$F$_z$ and LiPF$_6$ P-species as the contamination with weak intensity in XPS, which is corresponding to the EDX imaging of P in Figure S2.[26] Although the composition of SEI is similar to that of SEI formed in common electrolytes, there are some new compositions as shown in Li1s, N1s and Mn2p spectrum in Figure 1g. Li1s spectrum was fitted by ROCO$_2$Li, Li$_3$N, Li$_2$CO$_3$ and LiNO$_2$, where the peaks were located at 54.6, 55.0, 55.43 and 56.1 eV respectively. The N1s spectrum shows peaks of LiN$_x$O$_y$, Li$_3$N, and NO$_2^-$ locating at 397.6, 400.6, 403.9 eV respectively, in harmony with the Li1s spectrum and previous works.[28, 29] Note that the compositions of Li$_3$N and LiN$_x$O$_y$ are profitable for lithium anode because of their high Li-ion conductivity which can translate the large current density into ultralow local current density, leading to the uniform Li plating.[29] The homogeneous distribution of Li$_3$N, LiN$_x$O$_y$ and LiF that are important to stabilize the SEI layer, contributes the uniform and rapid lithium ion diffusion in SEI, giving rise to dendrite-free lithium deposition at high current density.[30-32] MnO$_x$ was probed by XPS which is in agreement with O1s spectrum and the result was further confirmed by Raman spectrum as shown in Figure S5.
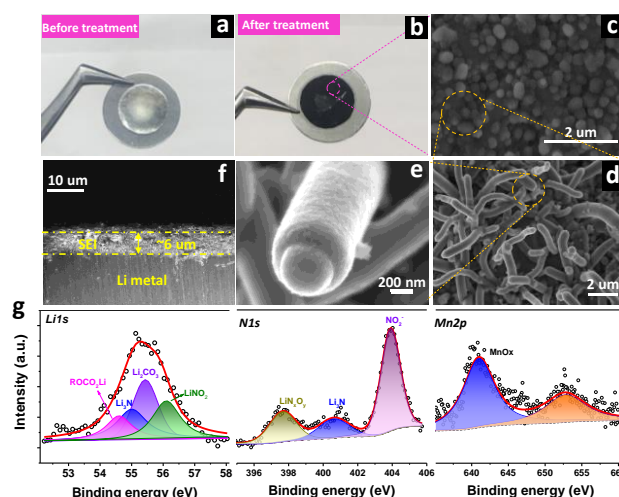

Figure 1. Pre-treated method, SEM imaging and XPS spectra of SEI. (a) Li metal on stainless steel without pre-treatment. (b) Li metal immersion in Mn(NO$_3$)$_2$ additive electrolyte within 1 min. (c) SEM imaging of SEI in (b). (d) Nanotubes morphology of the spherical shape in (c). (e) The zoom in figure of nanotube based on figure (d). (f) The cross-section of SEI in (b). (g) XPS spectra of SEI in (b) for the elements Li1s, N1s, and Mn2p.

To test the stability of SEI film formed in the electrolyte with additive, Li stripping/plating behavior was performed on a copper substrate. Bare Li anode was also performed for comparison. In two systems, Li was stripped from the anode and plated onto Cu electrode during discharge process and the process returned during charging. The contrast of potential profiles for the 1st, 50th and 100th cycle using different anodes are shown in Figure 2a, in which the blue line represents bare Li|Cu cell and the red line represents pretreated-Li|Cu cell, respectively. The current density was 3 mA cm^{-2} and the total discharge areal capacity was 6 mAh cm^{-2}. The overpotential reflects the nucleation barrier and the difference of overpotential is obvious with the increasing cycles. Note that the different electrochemical behaviour is completely dependent on Li anodes with or without pre-treatment, since the two cells present the same components such as Cu cathode, electrolyte and testing conditions apart from the Li anodes. The pretreated-Li|Cu cell kept stable electrochemical profile and low overpotential, demonstrating the uniform and stable SEI formed on the anode. The stable SEI insured more favorable Li plating kinetics and steady electrolyte environment, improving the Li stripping/plating behavior on Cu substrate in return. In contrast, in bare Li|Cu cell system, both the Cu substrate and the bare Li anode consumed Li ions and electrolyte to form the SEI. The unstable SEI blocked Li stripping/plating process and led to the increased resistance, giving rise to the higher overpotential. Moreover, the sustained consumption of Li ions and electrolyte caused by the unstable SEI resulted in the collapse of the cell eventually. The cycling performance with the coulombic efficiency of these two cells was also displayed, as shown in Figure 2b. The coulombic efficiency of pretreated-Li|Cu cell could be stabilized at ~ 94% over 150 cycles at a current density of 3 mA cm^{-2} and the areal capacity of 6 mAh cm^{-2}, showing the glorious stability of Li stripping/plating behavior. In comparison, bare Li|Cu cell exhibited inferior performance after 85 cycles, with rapid drop and low coulombic efficiency of ~ 0%. The unstable SEI in bare Li|Cu cell fostered the growth of Li dendrites, induced isolated Li particles and generated irreversible consumption of Li, accounting for the low coulombic efficiency and high overpotential. On the contrary, the good performance in pretreated-Li|Cu cell benefits from the stable SEI and the reasonable structure of SEI. The nanotubes arrays in SEI can redistribute the local electrical field and reduce the local current density, leading to the homogeneous Li deposition with less consumption of Li metal and electrolyte and improving the electrochemical behavior, which has been applied in previous report.[14]
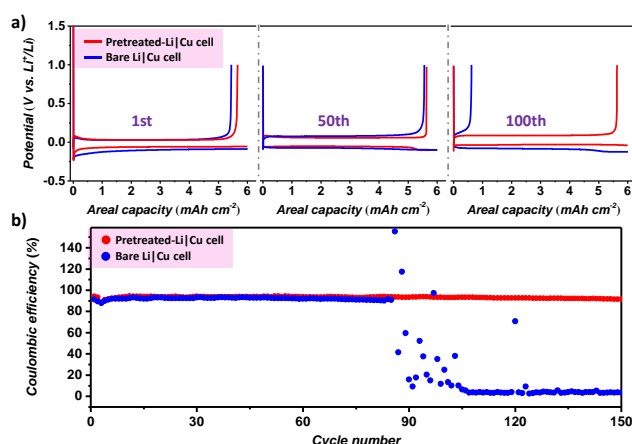

Figure 2. The contrast of Li stripping/plating performance of pretreated-Li|Cu cell and bare Li|Cu cell. (a) Voltage profiles of the Li stripping/plating on Cu substrate in the electrolyte of 1.0 M LiPF$_6$ in EC/DEC for the 1st, 50th and 100th cycle, respectively. (b) Cycling performance of pretreated-Li|Cu cell and bare Li|Cu cell. Both in (a) and (b), the current density is 3 mA cm^{-2} and areal capacity is 6 mAh cm^{-2}.

To further investigate the electrochemical performance of pretreated-Li electrode, galvanostatic stripping/plating behavior of the symmetric cell was explored. The current density was set to 1 mA cm^{-2} and the areal capacity was 1 mA h cm^{-2} with 30 s interval, as shown in Figure S6. The black line represents bare Li symmetric cell for comparison. The difference is not distinct when the current is small. Both symmetric cells show adjacent overpotential (~ 25 mV) for at least 300 hours. However, the profile of pretreated-Li symmetric cell is more stable than the other, because the overpotential of the latter is fluctuant even after hundreds of hours. The difference becomes apparent when the current density increases, as shown in Figure 3a. The current density was increased to 5 mA cm^{-2} with the areal capacity of 1 mA h cm^{-2}. For bare Li symmetric cell, the profile kept stable for only 100 hours with an overpotential of ~ 70 mV, after that the overpotential increased rapidly and eventually resulted in the cell failure after ~ 220 hours, demonstrating the nonuniform deposition of Li ions and irregular growth of dendrites. In contrast, the overpotential of the pretreated-Li symmetric cell could be stabilized as expected for over 500 hours, especially after 25 hours with a tiny overpotential of ~ 20 mV. In the first 25 hours, the SEI was in a gradient period with fluctuant overpotential which may be associated with the interfacial activation process, which could be also discovered in other works.[33-35] After the period, the symmetric cell shows a steady cycling behavior with tiny stable overpotential until the end of testing. With an increase in current density to 10 mA cm^{-2} and areal capacity to 2 mAh cm^{-2}, impressively, the pretreated-Li symmetric cell still maintains the stability of overpotential (~ 60 mV) for more than 500 hours with a same gradient period of the first 20 hours, as shown in Figure 3b. By contrast, the bare Li symmetric cell exhibited a fluctuant overpotential (~ 300 mV) the whole period and turned to failure after only 40 hours, demonstrating the frail interface. The rate performance of pretreated-Li symmetric cell was also investigated under the different current density of 5, 10, 15, and 20 mA cm^{-2} with the same charge/discharge time, as shown in Figure 3c. To reveal a

more evident evolution of the electrochemical behavior, the profiles of the middle two hours in every current density were enlarged. The stable overpotentials for each current density are 20, 40, 50, and 60 mV respectively. It is astonishing that the cell shows flat and stable overpotential profile even at an extremely high current density of 20 mA cm^{-2}. To the best of our knowledge, this is the first time to report an extremely high current density of 20 mA cm^{-2} with tiny overpotential compared with previous literature (see more details in Table S1). Benefit from the stable SEI and shunting effect (ensure the uniformly distributed Li ions) caused by the condensed nanotubes arrays on the surface of SEI in the pretreated-Li symmetric cell, the superior electrochemical behavior is achieved even at an extremely high current density. The SEM images of Li metal electrodes after cycles at the current density of 20 mA cm^{-2} (Figure S7) and the electrochemical impedance spectroscopy (EIS) measurements (Figure S8) also show the manifest difference which account for the different electrochemical performance. Notably, the random and asymmetric overpotential appears gradually during charging and discharging process with increasing current density. The probable reason could arise from the unavoidable asymmetry of the interface in two electrodes during pretreated operation. Furthermore, the electrochemical performance of the two cases with different SEI thickness in Figure S3 was also exhibited, please see more details in Figure S9.
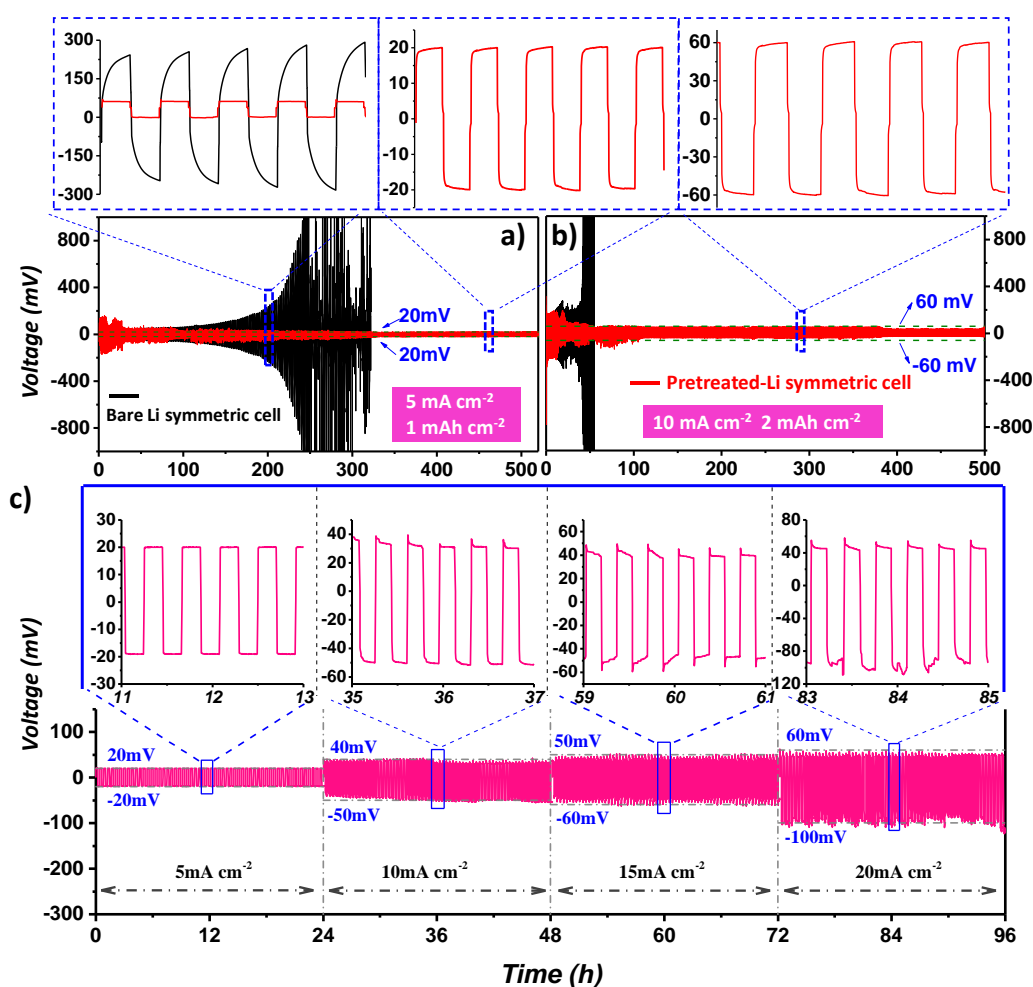

Figure 3. Galvanostatic stripping/plating performance of the pretreated-Li symmetric cell. (a) The comparison of the pretreated-Li symmetric cell (red line) and bare Li symmetric cell (black line) at the current of 5 mA cm^{-2} and areal capacity of 1 mAh cm^{-2}. (b) The comparison of the pretreated-Li symmetric cell (red line) and bare Li symmetric cell (black line) at the current of 10 mA cm^{-2} and areal capacity of 2 mAh cm^{-2}. (c) The rate performance of pretreated-Li symmetric cell at the rates of 5, 10, 15 and 20 mA cm^{-2}, respectively. The cell was tested after forming the stable SEI and the areal current was changed every 24 hours.

To explore the feasibility of pretreated-Li anode in the rigorous conditions for practical application, high-temperature test of pretreated-Li|LiMn$_2$O$_4$ and bare Li|LiMn$_2$O$_4$ full cells were performed at high rates. We chose the temperature of 55 ^{o}C and the rate of 2C (1C = 148 mA g^{-1}) since both of LiMn$_2$O$_4$ and lithium are sensitive to the high temperature at high rates due to the manganese dissolution and lithium dendrite. The 1st and 100th galvanostatic cycles of two cells are shown in Figure 4a and 4b. An evident difference can be seen comparing a rapid drop of specific capacity in bare Li|LiMn$_2$O$_4$ cell with a superior capacity retention of 87% at 100 cycles in pretreated-Li|LiMn$_2$O$_4$ cell. Figure 4c shows the cycling performance for the initial 200 cycles. The capacity descends quickly in initial cycles in bare Li|LiMn$_2$O$_4$ cell, meanwhile, the capacity retention reduced rapidly to less than 80% after 18 cycles. By contrast, the capacity retention is still larger than 82% for 200 cycles in

pretreated-Li|LiMn$_2$O$_4$ cell with an excellent cycling stability, demonstrating the evident improvement in the practical system caused by the pretreated-Li anode. The coulombic efficiency of the two cells is shown in Figure S10, which are deriving from Figure 4c. Pretreated-Li|LiMn$_2$O$_4$ cell maintains the flat and stable profile of coulombic efficiency for 200 cycles, including an increasing process in initial cycles. In comparison, bare Li|LiMn$_2$O$_4$ cell exhibits an analogous trend in initial cycles, after which the profile becomes fluctuant, demonstrating the unstable system. The rate performance at high temperature was also displayed, as shown in Figure S11. Two cells were tested at the different rates of 0.1C, 2C, 5C and 10C, respectively, after that the current density was returned to 0.1C. A manifest capacity decrease can be seen in bare Li|LiMn$_2$O$_4$ system, with the capacity of ∼ 60 mAh g^{-1} at 10C, compared with the capacity of ∼ 90 mAh g^{-1} in pretreated-Li|LiMn$_2$O$_4$ system. Moreover, the capacity resumed its original appearance with a high coulombic efficiency of 97.2% after returning the current density in pretreated-Li|LiMn$_2$O$_4$ system, demonstrating the stable and robust system. By contrast, the capacity only resumed to ∼ 75 mAh g^{-1} with a low coulombic efficiency of 56.7% in bare Li|LiMn$_2$O$_4$ system. Furthermore, a powerful recovery capability in capacity and coulombic efficiency can be seen in pretreated-Li|LiMn$_2$O$_4$ cell, as shown in Figure S12. The cells were performed at 10C rate in initial 5 cycles, after that the current density was returned to 0.1C with the high temperature. Pretreated-Li|LiMn$_2$O$_4$ cell exhibited a stable capacity of ∼ 90 mAh g^{-1} in 10C and responded rapidly to ∼ 110 mAh g^{-1} in 0.1C, companied by the increased coulombic efficiency from over 90% to ∼ 99% in initial 5 cycles and maintaining the coulombic efficiency at ∼ 99% in subsequent cycles without apparent fluctuation. In contrast, the capacity of bare Li|LiMn$_2$O$_4$ cell decreased fast from ∼ 60 mAh g^{-1} to ∼ 40 mAh g^{-1} in 10C and recovered to ∼ 70 mAh g^{-1} in 0.1C, far less than ∼ 110 mAh g^{-1} showed in pretreated-Li|LiMn$_2$O$_4$ cell. The coulombic efficiency was no more than 90% in initial 5 cycles, and with a sharp decrease to lower than 70% in subsequent cycles, displaying a remarkable difference compared with pretreated-Li|LiMn$_2$O$_4$ cell. The distinct improvement is directly traceable to the stable and efficient SEI, which reduces the local current density and generates homogenous Li$^+$ flux distribution.
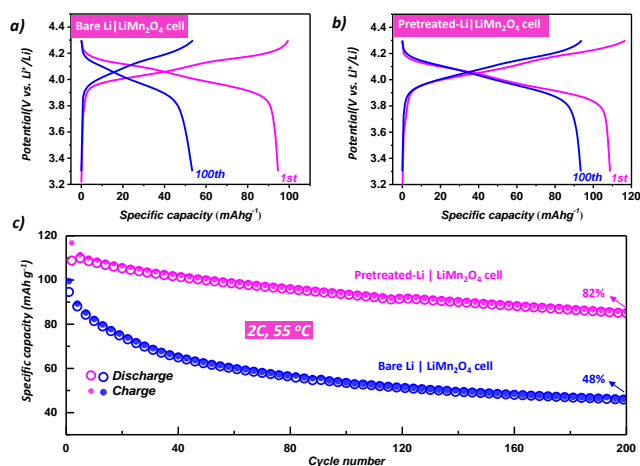

Figure 4. Cell performance comparison between bare Li|LiMn$_2$O$_4$ cell and pretreated-Li|LiMn$_2$O$_4$ full cells. Typical galvanostatic profiles of (a) bare Li|LiMn$_2$O$_4$ cell and (b) Pretreated-Li|LiMn$_2$O$_4$ cell for the 1st and 100th cycle, respectively, at the 2C rate (1C = 148 mA g^{-1}) and 55 °C high temperature. (c) Cycling performance of bare Li|LiMn$_2$O$_4$ cell and pretreated-Li|LiMn$_2$O$_4$ cell at 2 C and 55 °C. The potential window was set to 3.3 ∼ 4.3 V.

Conclusions

In summary, we construct an artificial organic/inorganic protective layer for typical lithium anodes via pre-treatment in Mn(NO$_3$)$_2$-containing carbonate electrolyte, remarkably stabilizing the Li plating/stripping behaviour during ultrafast charge-discharge cycling. The as-prepared SEI composed by unique nanotubes arrays could effectively suppress the growth of dendrites and refrain the unstable interface, thereby performing minimized overpotential at an ultrahigh rate. In symmetric cell tests, the overpotential is as small as 20 mV at 5 mA cm^{-2} over 500 hours, in stark contrast to the rapid failure in bare Li cell. Moreover, pretreated-Li cell reduces the overpotential to ∼ 60 mV at an extremely high current of 20 mA cm^{-2}. In the practical system, pretreated-Li|LiMn$_2$O$_4$ cell shows outstanding performance with 83% capacity retention over 200 cycles at a high rate of 2C and a high temperature of 55 °C. Furthermore, the cell demonstrates a robust recovery capability with high capacity and coulombic efficiency after the cycles at 10C. The strategy of pretreating lithium metal shows high efficiency and good electrochemical performance especially at high current density. More important, the operation is facile and immediate with low consumption. We expect our work to inspire the new way for the design of Li-metal anodes, and thereby facilitate the development and the practical utilization of Li-metal batteries.

Acknowledgment

Notes and references

The authors declare no competing financial interests.

1.   S. Guo, Q. Li, P. Liu, M. Chen and H. Zhou, *Nat. Commun.,* 2017, 8, 135.
2.   S. Guo, P. Liu, H. Yu, Y. Zhu, M. Chen, M. Ishida and H. Zhou, *Angew. Chem. Int. Ed.,* 2015, 54, 5894.
3.   X. Li, Y. Qiao, S. Guo, Z. Xu, H. Zhu, X. Zhang, Y. Yuan, P. He, M. Ishida and H. Zhou, *Adv. Mater.,* 2018, 30, 1705197.
4.   P. G. Bruce, S. A. Freunberger, L. J. Hardwick and J.-M. Tarascon, *Nat. Mater.,* 2012, 11, 19.
5.   W. Xu, J. Wang, F. Ding, X. Chen, E. Nasybulin, Y. Zhang and J.-G. Zhang, *Energy Environ. Sci.,* 2014, 7, 513.
6.   S. Bai, X. Liu, K. Zhu, S. Wu and H. Zhou, *Nat. Energy,* 2016, 1, 16094.
7.   S. Wu, J. Tang, F. Li, X. Liu, Y. Yamauchi, M. Ishida and H. Zhou, *Adv. Funct. Mater.*, 2016, 26, 32910.
8.   Y. Qiao, S. Wu, J. Yi, Y. Sun, S. Guo, S. Yang, P. He and H. Zhou, *Angew. Chem. Int. Ed.,* 2017, 56, 4960.
9.   F. Qiu, X. Zhang, Y. Qiao, X. Zhang, H. Deng, T. Shi, P. He and H. Zhou, *Energy Storage Mater.,* 2018, 12, 176.
10.   X. B. Cheng, R. Zhang, C. Z. Zhao, F. Wei, J. G. Zhang and Q. Zhang, *Adv. Sci.,* 2016, 3, 1500213.
11.   Y. Lu, S. K. Das, S. S. Moganty and L. A. Archer, *Adv. Mater.,* 2012, 24, 4430.
12.   H. Ye, S. Xin, Y.-X. Yin, J.-Y. Li, Y.-G. Guo and L.-J. Wan, *J. Am. Chem. Soc.,* 2017, 139, 5916.
13.   T. T. Zuo, X. W. Wu, C. P. Yang, Y. X. Yin, H. Ye, N. W. Li and Y. G. Guo, Adv. Mater., 2017, 29, 1700389.
14.   D. Lin, Y. Liu and Y. Cui, *Nat. Nanotech.,* 2017, 12, 194.
15.   S. Liu, X. Xia, Y. Zhong, S. Deng, Z. Yao, L. Zhang, X. B. Cheng, X. Wang, Q. Zhang and J. Tu, *Adv. Energy Mater.*, 2018, 8, 1702322.
16.   Y. H. Zhang, J. F. Qian, W. Xu, S. M. Russell, X. L. Chen, E. Nasybulin, P. Bhattacharya, M. H. Engelhard, D. H. Mei, R. G. Cao, F. Ding, A. V. Cresce, K. Xu and J. G. Zhang, *Nano Lett.,* 2014, 14, 6889;
17.   F. Ding, W. Xu, X. Chen, J. Zhang, Y. Shao, M. H. Engelhard, Y. Zhang, T. A. Blake, G. L. Graff and X. Liu, *J. Phys. Chem. C*, 2014, 118, 4043.
18.   B. Zhu, Y. Jin, X. Hu, Q. Zheng, S. Zhang, Q. Wang and J. Zhu, *Adv. Mater.,* 2017, 29, 1603755.
19.   C. Sun, J. Liu, Y. Gong, D. P. Wilkinson and J. Zhang, *Nano Energy*, 2017, 33, 363.
20.   Y. Y. Liu, D. C. Lin, Z. Liang, J. Zhao, K. Yan and Y. Cui, *Nat. Commun.,* 2016, 7,10992.
21.   H. L. Yu, J. N. Zhao, L. B. Ben, Y. J. Zhan, Y. D. Wu and X. J. Huang, *ACS Energy Lett.,* 2017, 2, 1296.
22.   R. Xu, X. Q. Zhang, X. B. Cheng, H. J. Peng, C. Z. Zhao, C. Yan and J. Q. Huang, *Adv. Funct. Mater.,* 2018, 28, 1705838.
23.   S. Choudhury, R. Mangal, A. Agrawal and L. A. Archer, *Nat. Commun.,* 2015, 6, 10101.
24.   L. Liu, Y.-X. Yin, J.-Y. Li, N.-W. Li, X.-X. Zeng, H. Ye, Y.-G. Guo and L.-J. Wan, *Joule*, 2017, 1, 563.
25.   B. S. Parimalam, A. D. MacIntosh, R. Kadam and B. L. Lucht, *J. Phys. Chem. C*, 2017, 121, 22733.
26.   M. Nie, D. Chalasani, D. P. Abraham, Y. Chen, A. Bose and B. L. Lucht, *J. Phys. Chem. C,* 2013, 117, 1257.
27.   F. Ding, W. Xu, D. Choi, W. Wang, X. Li, M. H. Engelhard, X. Chen, Z. Yang and J.-G. Zhang, *J. Mater. Chem.,* 2012, 22, 12745.
28.   S. Xiong, K. Xie, Y. Diao and X. Hong, *Electrochim. Acta,* 2012, 83, 78.
29.   J. Guo, Z. Wen, M. Wu, J. Jin and Y. Liu, *Electrochem. Commun.,* 2015, 51, 59.
30.   X. B. Cheng, T. Z. Hou, R. Zhang, H. J. Peng, C. Z. Zhao, J. Q. Huang and Q. Zhang, *Adv. Mater.,* 2016, 28, 2888;
31.   X. Q. Zhang, X. Chen, X. B. Cheng, B. Q. Li, X. Shen, C. Yan, J. Q. Huang and Q. Zhang, *Angew. Chem. Int. Ed.,* 2018, 57, 1-6;
32.   Y. Lu, Z. Tu and L. A. Archer, *Nature Mater.*, 2014, 13, 961.
33.   X. X. Zeng, Y. X. Yin, N. W. Li, W. C. Du, Y. G. Guo and L. J. Wan, *J. Am. Chem. Soc.,* 2016, 138, 15825;
34.   A. Basile, A. I. Bhatt and A. P. O'Mullane, *Nat. Commun.,* 2016, 7, 11794;
35.   R. Miao, J. Yang, X. Feng, H. Jia, J. Wang and Y. Nuli, *J. Power Sources,* 2014, 271, 291.